

# Charge-compensated, semiconducting single-walled carbon nanotube thin film as an electrically configurable optical medium

Feihu Wang<sup>1,2</sup>, Mikhail E. Itkis<sup>1,3</sup>, Elena Bekyarova<sup>1,3</sup> and Robert C. Haddon<sup>1,2,3,4</sup>\*

**A two-terminal semiconducting single-walled carbon nanotube (SC-SWNT) film in contact with an ionic liquid allows the realization of an extremely high density of holes, inducing a strong position-dependent electromodulation of the interband and excitonic transitions as a result of the position-dependent shift of the SWNT Fermi level. Electrical control of the optical transmission suggests applications of the SC-SWNT thin films as electrically configurable optical media, while the wide spectral range of the electro-optical modulation, which extends from the far-infrared to the visible, provides a viable approach to large-area electrochromic smart windows.**

Single-walled carbon nanotubes (SWNTs) have unique optoelectronic properties due to their one-dimensional electronic structure<sup>1–3</sup>. A number of photonic applications have been proposed based on the observation of photodetection and light emission from SWNTs<sup>3–12</sup>, and SWNT thin films have been explored as transparent conducting coatings in large-area solar cells and displays<sup>13–17</sup>. Electro-optical phenomena provide another fascinating but less explored field of SWNT photonics. Most reports of this relate to the modulation of the interband and excitonic transitions in SWNT thin-film field-effect transistors (FETs), making use of electrolytic cells and solid-state gates<sup>13,18–20</sup>, and the search for the theoretically predicted enhancement of Frank–Keldysh and Stark effects<sup>3,21</sup> is still in progress<sup>20,22–24</sup>.

In this Article, we report a simple two-terminal semiconducting (SC) SWNT thin-film device, which, when in contact with an ionic liquid, allows the realization of an extremely high density of holes, inducing a strong electromodulation of the interband and excitonic transitions as a result of the position-dependent shift of the SWNT Fermi level. The wide spectral range of the electro-optical modulation, which extends from the far-infrared to the visible, recommends the application of this technology to electrochromic smart windows for energy-efficient buildings and vehicles<sup>25–28</sup>.

In this study, we used a simple two-terminal device with gold contacts fabricated on optical substrates, in which the active channel consisted of a film of semiconducting SWNTs (SC-SWNTs; see Methods). After device preparation, the annealed SWNT channel showed a linear current–voltage ( $I$ – $U$ ) relationship (Fig. 1a), and we observed no change in the optical transparency of the films under an applied voltage. However, after application of a thin layer of *N,N*-diethyl-*N*-(2-methoxyethyl)-*N*-methylammonium bis-(trifluoromethylsulfonyl)-imide (DEME-TFSI) ionic liquid to the SWNT channel, the  $I$ – $U$  characteristics became strongly nonlinear (Fig. 1a), with the resistance decreasing by an order of magnitude at the highest applied voltage. In addition, we observed a strong modulation of the infrared transmission (Fig. 1b), with the strongest electromodulation observed in the vicinity of the current injection electrode at a wavelength of 1.8  $\mu\text{m}$ , which corresponds to the first absorption band of SC-SWNTs ( $S_{11}$ ) of average diameter

1.55 nm (ref. 20). The amplitude and sign of the electro-optical effect changed with the amplitude and polarity of the applied voltage (Fig. 1b) as well as with the position of the infrared beam along the channel (see below).

We used a prepatterned optical substrate with 20 in-line electrodes (Fig. 1c) to study the spatial distribution of the electrical potential  $U$  along the SWNT channel as a function of applied voltage (see Methods). The experimental set-up was tested on a SC-SWNT sample before application of the ionic liquid and showed a linear distribution of electrical potential  $U(x)$  along the SWNT channel (Fig. 1d) and no indication of detectable electro-optical effects. The  $U(x)$  distribution as a function of the amplitude and polarity of the applied voltage after immersing the SWNT channel in a thin layer of ionic liquid is shown in Fig. 1e. With increasing voltage we observe an upward bending of the  $U(x)$  curve, with the formation of a high electric field region in the vicinity of the negative electrode. At the highest applied voltage,  $U = 2.5$  V, the high electric field region compresses to a segment  $<30$   $\mu\text{m}$  wide. The strength of the electric field at the negative current contact reached  $500$   $\text{V cm}^{-1}$ , exceeding the strength of the field at the positive contact by more than two orders of magnitude. On reversing the device polarity the high field region shifted to the opposite contact (Fig. 1e). The temporal evolution of the electrical potential distribution along the channel is presented in the inset to Fig. 1e, and shows a time constant of  $\sim 100$  ms for the formation of the strongly nonlinear potential profile.

A schematic of the experiments is presented in Fig. 2a, together with the electro-optical near-infrared response of the film as a function of position along the SWNT channel. Figure 2b–d shows the absorption spectra in the segments of the SWNT film adjacent to the negative and positive electrodes (positions A and C, respectively) and at the central position B. In the absence of an applied voltage ( $U = 0$ ), the absorption spectrum shows a position-independent  $S_{11}$  peak that is partially suppressed due to residual environmental doping. At the negative current contact (position A), the application of a voltage leads to a slight enhancement of the  $S_{11}$  peak as the film approaches its intrinsic state. At the positive electrode (position C) there is a strong suppression of the  $S_{11}$  peak and the  $S_{11}$  feature

<sup>1</sup>Center for Nanoscale Science and Engineering, University of California – Riverside, Riverside, California 92521, USA, <sup>2</sup>Department of Physics and Astronomy, University of California – Riverside, Riverside, California 92521, USA, <sup>3</sup>Department of Chemistry, University of California – Riverside, Riverside, California 92521, USA, <sup>4</sup>Department of Physics, King Abdulaziz University, Jeddah 21589, Saudi Arabia. \*e-mail: haddon@ucr.edu

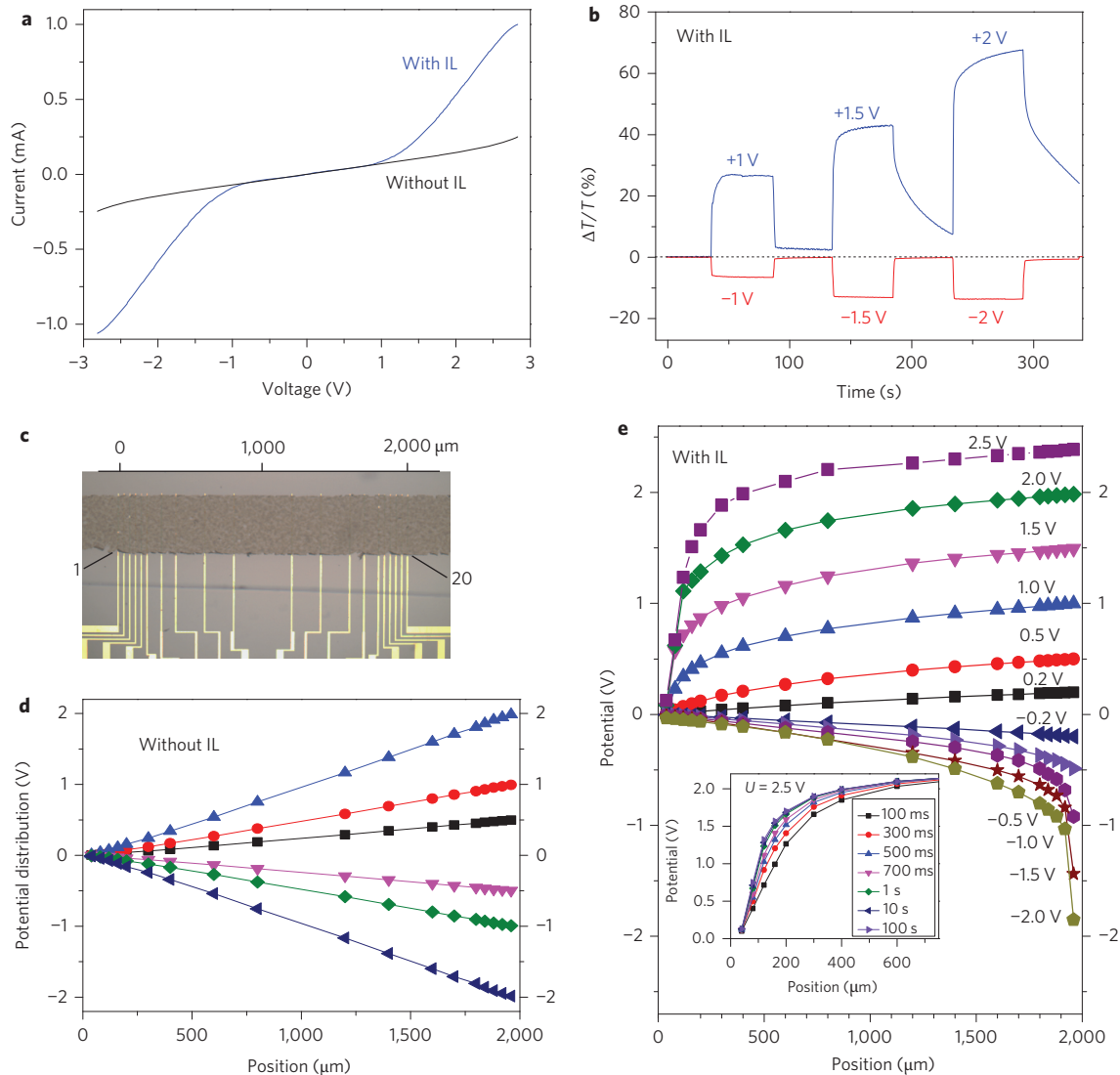


**Figure 1 | Nonlinear electrical and electro-optical behaviour of a SC-SWNT film coated with ionic liquid.** **a**, Nonlinear  $I$ - $U$  characteristics of an SWNT thin-film channel after coating with ionic liquid (IL). **b**, Electromodulation of infrared transmittance  $\Delta T/T$  at a wavelength of  $1.8\ \mu\text{m}$  as a function of the amplitude and polarity of the applied voltage in the vicinity of the current-injecting electrode. **c**, Configuration of the SC-SWNT film on a prepatterned substrate with 20 in-line electrodes. **d**, Linear spatial distribution of the electrical potential  $U(x)$  along the SWNT channel before coating with ionic liquid. **e**, Nonlinear spatial distribution of the electrical potential along the SWNT channel after coating with ionic liquid as a function of the amplitude and polarity of the applied voltage. The values of the applied voltage are shown next to the corresponding  $U(x)$  curves. Inset: temporal evolution of the electrical potential distribution at  $U = 2.5\ \text{V}$ .

completely disappears at  $U = 2\ \text{V}$ ; a further increase of the voltage leads to the complete suppression of the  $S_{22}$  peak and the appearance of a new peak located between the initial  $S_{11}$  and  $S_{22}$  transitions, which was first observed in 1998 under extreme iodine doping of soluble SWNTs<sup>29</sup>, and recently rediscovered and ascribed to a three-particle excited state<sup>30</sup>. The central part of the sample shows the same behaviour as is observed at the positive electrode, but with smaller amplitude.

The spatially resolved distribution of the electromodulation of the infrared transmission ( $\Delta T(U, x)/T_{U=0V}(\%)$ ), at a fixed wavelength of  $1.8\ \mu\text{m}$  is presented in Fig. 2e,f as a function of amplitude and the polarity of the applied voltage. With the application of a voltage, a region of slightly decreasing infrared transmittance develops near the negative electrode, while the transmittance in the vicinity of the positive electrode strongly increases. With further increase of voltage the region of increasing transmittance asymmetrically expands to occupy most of the channel length, while the region of negative electro-transmittance remains localized within  $50\ \mu\text{m}$  of

the negative electrode (Fig. 2e). Interchange of the contact polarities leads to an inversion of the sign of the electromodulation at the electrodes, while the transmittance (measured at a wavelength of  $1.8\ \mu\text{m}$ ) in the central region of the SWNT channel remains positive and independent of the polarity of the applied voltage (Fig. 2e-g). The strong electromodulation of the SWNT thin-film interband absorption features resembles the effects observed in electrolyte gated devices used in previous spectro-electrochemistry experiments<sup>18,19</sup>, although our two-terminal devices do not make use of a gate electrode.

The SWNT network is treated as a semiconducting medium and the band structure in relationship to the charge distribution in the ionic liquid is presented in Fig. 3. In the absence of the ionic liquid (at  $U = 0\ \text{V}$ , Fig. 3a), the interconnected SWNT network can be described by a position-independent Fermi level  $E_F$ ; the relationship of the Fermi level to the positions of the valence (V) and conduction (C) bands does not change under an applied voltage, so all the bands and the local chemical potential line acquire the slope  $dU/dx$  (Fig. 3b), as confirmed by the linear

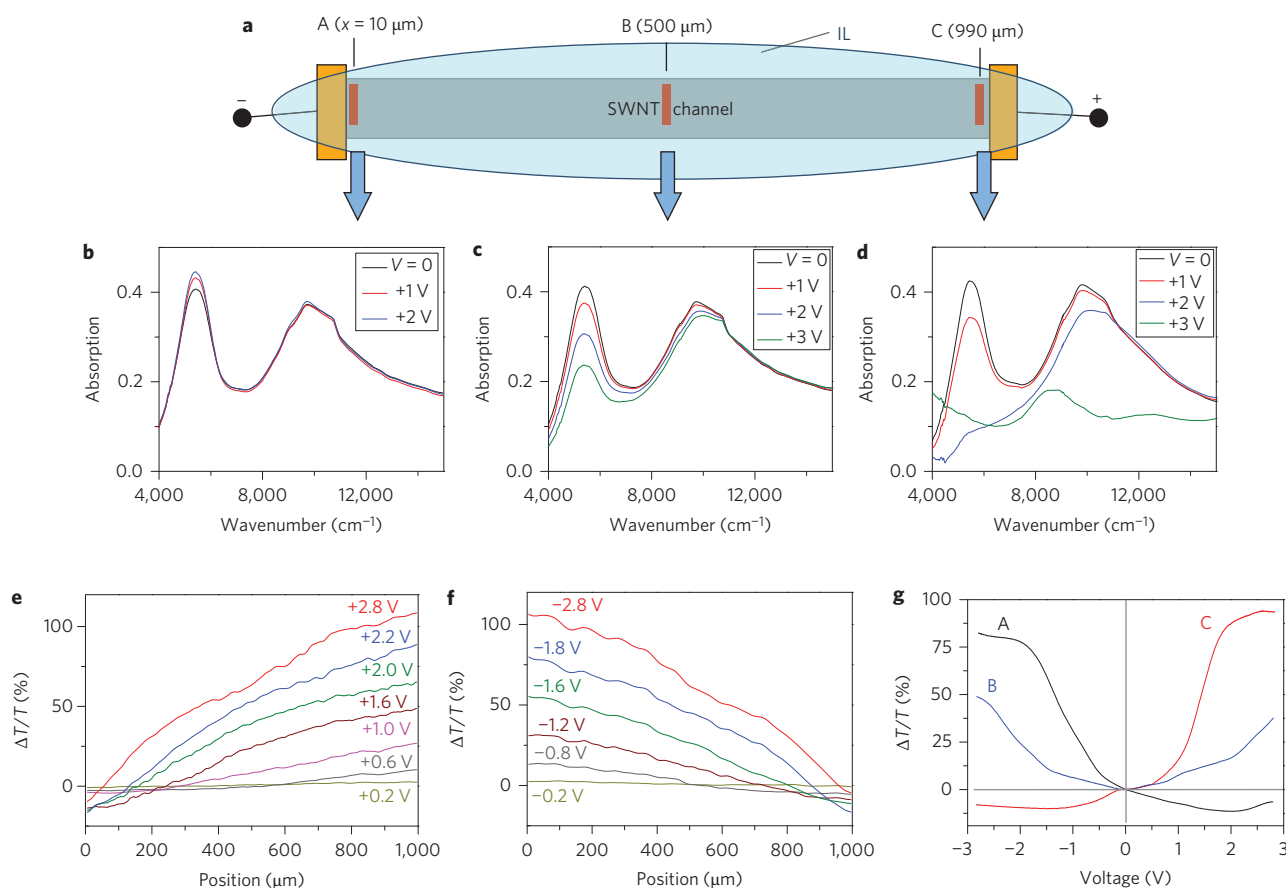


**Figure 2 | Spatial distribution of the electro-optical effect in the SC-SWNT thin-film channel in ionic liquid.** **a**, Schematic of the set-up for electro-optical measurement with the narrow infrared beam scanning the length of the SWNT channel. **b–d**, Modification of the absorption spectra of the SWNT film at negative and positive electrodes (positions A and C, respectively) and the centre of the channel (position B). **e, f**, Spatial dependence of the electromodulation of infrared transmittance  $\Delta T/T$  on the amplitude and polarity of the applied voltage measured at a wavelength of  $1.8 \mu\text{m}$ . **g**, Voltage dependence of  $\Delta T/T$  at different positions along the SWNT channel measured at a wavelength of  $1.8 \mu\text{m}$ .

potential distribution presented in Fig. 1d ( $U \neq 0$  V). It is well known that gold makes p-type contacts to SC-SWNTs and that the Fermi level is pinned near the top of the valence band as a result of the high workfunction of the gold electrode, hole doping of the SC-SWNTs, and the contact geometry<sup>31–35</sup>.

In the presence of the ionic liquid at zero voltage, the DEME<sup>+</sup> cations and TFSI<sup>-</sup> anions are distributed uniformly along the surface of the SWNT film (Fig. 3c), with the local value of  $E_F$  independent of position along the channel, as confirmed by the position-independent absorption spectra (Fig. 2b–d). Following application of a voltage, anions and cations are separated, generating a high concentration of cations in the vicinity of the negative electrode and anions at the positive electrode, thereby forming a lateral electric double-layer capacitor (Fig. 3d)<sup>36–41</sup>. This spatial redistribution of ions shifts the local Fermi level in the carbon nanotube network in different directions at the two electrodes: down in energy towards the highly p-doped state at the positive electrode (as confirmed by the strong suppression of the  $S_{11}$  absorption band), and up in energy at the negative electrode towards the intrinsic state (as indicated by the slightly increasing  $S_{11}$  absorption). It should be noted that the depletion of the valence band will suppress the optical absorption features independent of their single-particle or excitonic nature. The final distribution of the electrical potential along the SWNT channel is established through the equilibration of the ionic and SWNT charge distribution as determined by the position-dependent shift of the Fermi level. This distribution is presented schematically in Fig. 3d. The highly resistive region of the

channel in the vicinity of the negative electrode, which constitutes the intrinsic state, experiences most of the potential drop, resulting in the high electric field, as can be seen in Fig. 1.

Given the p-type nature of the device, it can be envisioned as two rectifying metal–semiconductor junctions biased in opposite directions and connected in series, one operating under forward bias at the hole-injecting positive contact, and the other operating under reverse bias at the negative contact. We suggest that the polarized distribution of cations and anions in the ionic liquid functions in the same manner as the ionized donor and acceptor sites in the channel of a heavily doped semiconductor. The space charge set-up in the ionic liquid is external to the lattice of SWNTs, in contrast to the situation for ionized donors and acceptors in conventional semiconductors, but it is very effective because of the geometry of the SWNT network, which allows the ions to diffuse into close proximity to the SWNT walls within the galleries between SWNTs. It can be dynamically adjusted in response to the applied voltage and the charge injected into the SWNT channel. In related experiments, the use of the ionic liquid DEME–TFSI as a polarizable medium allowed the observation of superconductivity in such insulators as SrTiO<sub>3</sub> and ZrNCl, as well as the efficient gating of ZnO, Bi<sub>2</sub>Te<sub>3</sub> and graphene FET channels<sup>36–41</sup>.

The bandgap in SC-SWNTs is inversely proportional to the SWNT diameter and, for smaller-diameter SWNTs, the  $S_{11}$  absorption band is shifted to higher energies (Fig. 4a). The same basic relationship between the positions of the absorption features and the SWNT diameter should be valid where the absorption originates

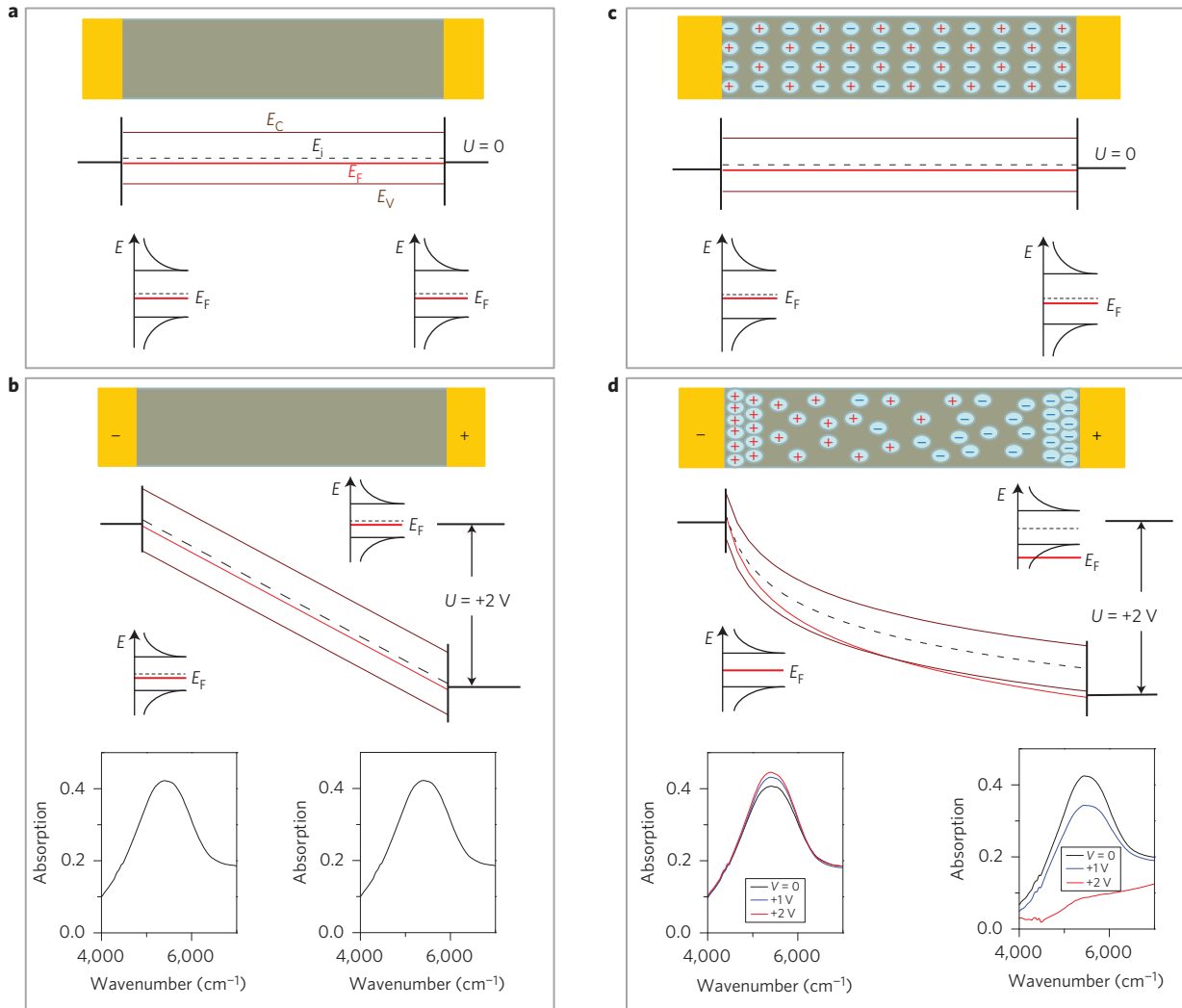


**Figure 3 | Model of observed nonlinear electrical and electro-optical effects in SWNT thin films in ionic liquid.** **a,b**, Spatial distribution of the SWNT valence and conduction bands, Fermi level and electronic density of states (DOS) in the SWNT channel without ionic liquid (**a**,  $U = 0$  V; **b**,  $U = 2$  V). **c,d**, Spatial distribution of cations and anions in the ionic liquid, SWNT valence  $E_V$  and conduction  $E_C$  bands (brown lines), Fermi level  $E_F$  (red line), neutrality  $E_i$  (middle of the gap; dashed line), and DOS in the SWNT channel coated with ionic liquid (**c**,  $U = 0$  V; **d**,  $U = 2$  V). The plots in **b** and **d** show the  $S_{11}$  transition absorption band under applied voltage in the vicinity of electrodes with ionic liquid (**b**) and without ionic liquid (**d**).

from excitonic excitations and the spectral weight is shifted due to strong electron–hole interaction in the one-dimensional SWNTs. To explore the spectral range of the electro-optical modulation, we fabricated a set of gated electro-optical devices in which the channels were composed of SWNTs with four different average diameter distributions:  $D_{av} = 1.55 \pm 0.1$  nm,  $1.3 \pm 0.1$  nm,  $1.0 \pm 0.2$  nm and  $0.8 \pm 0.1$  nm. The transparent gate electrodes comprised a thin film of 99% metallic SWNTs, with a thin layer of ionic liquid separating the electro-active SC-SWNT channel from the transparent gate electrode, as shown schematically in Fig. 4b. Figure 4c shows the strong electromodulation of the transmittance for all the devices, which involves both  $S_{11}$  and  $S_{22}$  bands, and the electromodulated spectra extend from the near-infrared to the visible (2,500 nm to 500 nm).

Shifting the Fermi level below the top of the valence band not only suppresses the  $S_{11}$  and  $S_{22}$  interband transitions but also produces free carrier excitations (transitions  $S_{fc}$ , Fig. 4a), which absorb in the mid- and far-infrared spectral ranges. Figure 4d shows the transfer of the spectral weight from the near-infrared  $S_{11}$  absorption to the mid- and far-infrared range, which includes the 3–5  $\mu\text{m}$  and  $\sim 10$   $\mu\text{m}$  atmospheric transparency bands.

Recently, electrochromic materials (materials that can change their optical properties under an applied voltage) have emerged as a promising technology for engineering smart windows that are capable of reducing the heating and cooling loads and increasing the lighting efficiency in buildings<sup>25–27</sup>, as well as improving thermal control and reducing fuel consumption in vehicles<sup>28</sup>. Carbon nanotubes have been considered in electrochromic smart window design for use in transparent conducting electrodes, replacing indium tin oxide<sup>13–17,26</sup>. This current study, together with earlier developments<sup>13,18–20</sup>, suggests that SWNTs could contribute to this technology as an active electrochromic layer in smart window applications.

Figure 5 provides some alternative configurations for our SWNT thin-film-based electro-optical devices. Figure 5a presents a schematic of a SWNT electro-optical modulator in which the voltage is applied between two closely situated electrodes and allowed to uniformly switch the optical transparency of the large area of the device external to the contacts. Figure 5c illustrates the experimental realization of this configuration and shows the transmission data for such a device as a function of applied voltage and position. Figure 5b presents a schematic of another SWNT thin-film-based

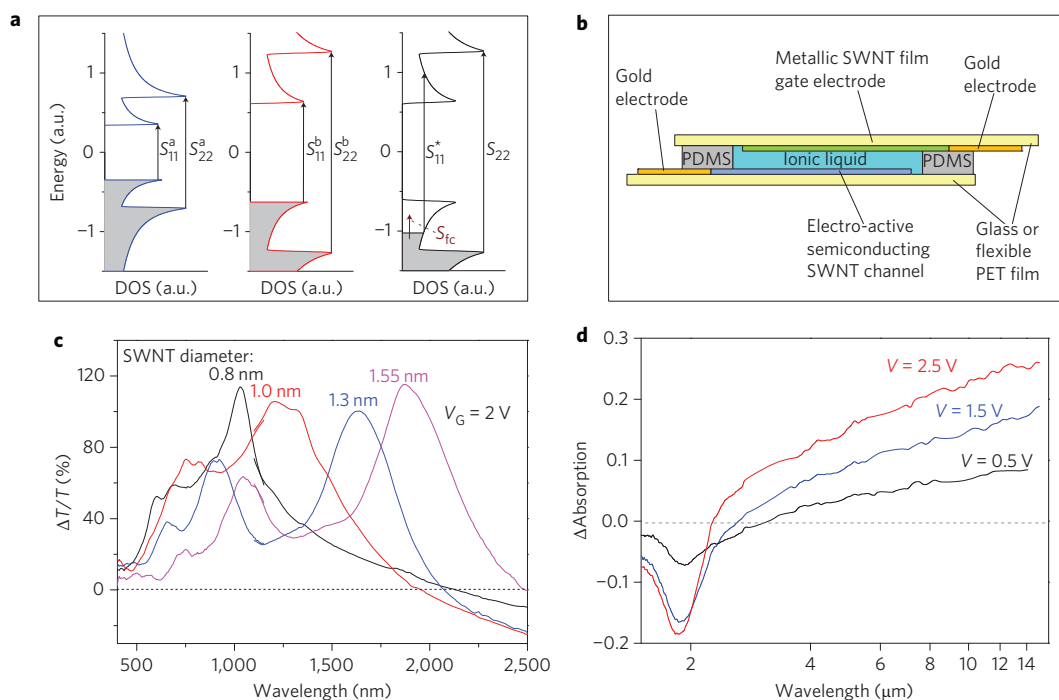


**Figure 4 | Spectral range of electro-optical effects in SWNT thin films in ionic liquid.** **a**, Electronic density of states (DOS) of SC-SWNTs of larger diameter/smaller bandgap (left); smaller diameter/larger bandgap (centre); and in the case of the shift of the chemical potential inside the valence band leading to the suppression of interband transitions  $S_{11}$  and  $S_{22}$  and the appearance of low-energy free-carrier absorption  $S_{fc}$  (right). **b**, Schematic of electro-optical field-effect transistor (EO-FET) with SC-SWNTs as the electro-active channel and metallic SWNTs as the gate electrode, separated by a layer of ionic liquid. **c**, Electromodulation of transmission  $\Delta T/T$  using EO-FETs with SC-SWNTs of four different diameters from 0.8 nm to 1.55 nm, with the spectra of electromodulation extending from the visible to near-infrared (500–2,500 nm). **d**, Electromodulation of  $S_{11}$  absorption accompanied by modulation of mid- and far-infrared absorption originating from  $S_{fc}$  excitations.

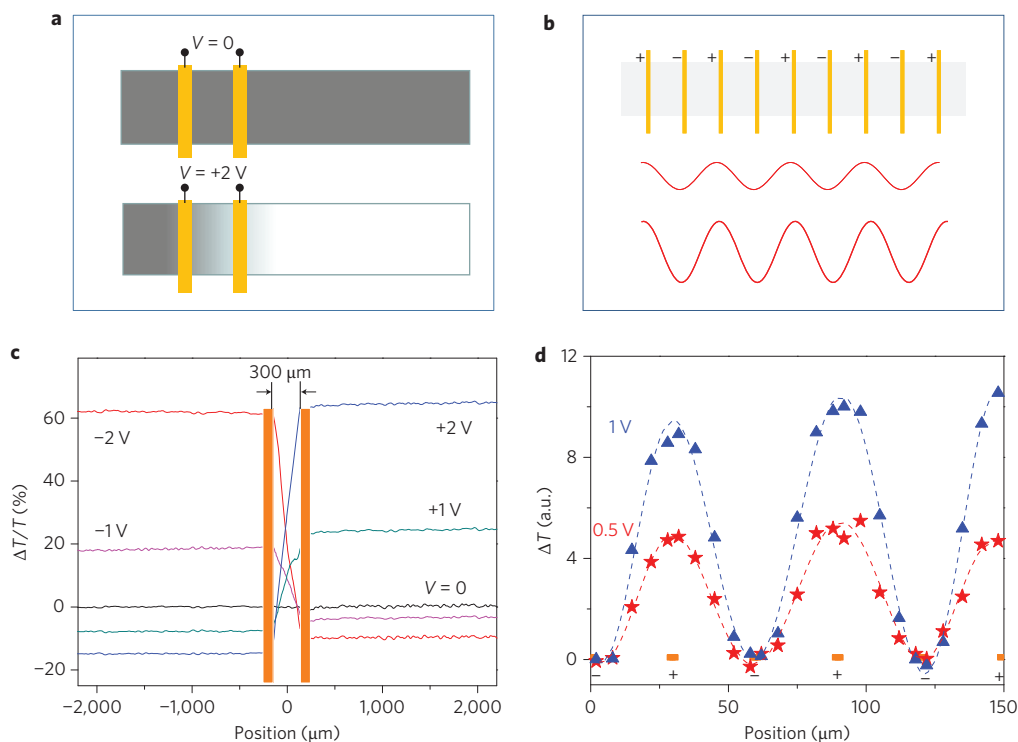


**Figure 5 | Electro-optical configuration and functionalities based on the SWNT thin-film channel in an ionic liquid.** **a, c**, Schematic of set-up (**a**) in which a large area of SWNT film can be switched from an opaque to the transparent state by application of voltage across two closely separated electrodes, and its experimental demonstration (**c**). **b, d**, Schematic (**b**) of a set of interdigitated electrodes inserted in the SWNT channel to be used to generate periodic spatial electromodulation of infrared transmittance (with the amplitude and phase controlled by the amplitude and polarity of the applied voltage) and experimental demonstration (**d**).

electro-optical functionality in which a set of interdigitated electrodes is inserted along the channel. Under application of a voltage, a periodic spatial modulation of transmittance can be produced, with the amplitude and phase controlled by the amplitude and polarity of the applied voltage, as experimentally demonstrated in Fig. 5d. The spatial modulation of the transmittance presented in Fig. 5c,d was conducted at a wavelength 1.8  $\mu\text{m}$ , but the spectral range of modulation can also be extended to mid- and far-infrared wavelengths, as shown in Fig. 4d. The period of modulation can also be changed by addressing different groups of electrodes; such a system can be used as an electrically configurable diffraction grating for an infrared spectrophotometer, where the wavelength can be scanned without moving parts.

In summary, we have demonstrated that the application of an electrical potential to a SC-SWNT film in the presence of an ionic liquid leads to a position-dependent modulation of the optical transmission, which is associated with the injection of holes into the SC-SWNT valence band, dynamically compensated by the polarized medium of the ionic liquid. The electrical control of the local optical transmission suggests the applications of SC-SWNT thin films as electrically configurable optical media. The broad spectral range of electro-optical modulation, which extends from the far-infrared to the visible, suggests that the SWNT thin films are candidate materials for utilization as the active layer in electrochromic smart windows.

## Methods

SWNT thin films were prepared by vacuum filtration<sup>20</sup> and transferred to optical substrates with prepatterned Cr(10 nm)/Au(100 nm) electrodes to form rectangular channels of length 1,000–2,000  $\mu\text{m}$  and width 200–400  $\mu\text{m}$ . Before measurement, the SWNT films were annealed in vacuum to reduce the effect of environmental doping. The thickness of the SWNT films was kept in the range 40–100 nm by controlling the amount of SWNT material utilized in the vacuum filtration. A Dektak profilometer was used to obtain the final film thickness, after calibration by carrying out measurements on thick SWNT films. A thin film frame of poly(dimethylsiloxane) (PDMS, thickness of  $\sim 200 \mu\text{m}$ ) was placed around the SWNT channel to contain a thin uniform layer of ionic liquid. After filling the frame, the ionic liquid was covered with a sapphire window. Flexible structures were also fabricated with Mylar films. To study the spatial distribution of the electrical potential  $U$  along the SWNT channel, a 20 in-line electrode configuration (Fig. 1c) was used. The electrodes were 3  $\mu\text{m}$  wide and more densely populated in the vicinity of the current contacts where the separation between the electrodes was 20–40  $\mu\text{m}$ , thus defining the spatial resolution. The current was applied between contacts 2 and 19 (numbered in order from left to right in Fig. 1c), so contacts 1 and 20 measured the potential under the current-injecting electrodes, excluding the contact contribution, using a Keithley 2700 multichannel data acquisition system. For spatially resolved electro-optical measurements, the two-electrode configuration was used. The infrared beam from the monochromator (Horiba Yobin-Robin ihr 320) was focused into a narrow 10- $\mu\text{m}$ -wide strip (Fig. 2a) using an infrared microscope (Bruker Hyperion 1000). The sample was mounted on a motorized micrometer stage so that the electro-optical response could be acquired along the length of the SWNT channel. The sign and amplitude of the electro-optical response were measured using the two-frequency modulation technique with two lock-in amplifiers (SRS 830) to analyse the response. The infrared radiation was chopped at a frequency of 200–400 Hz and the voltage across the channel was applied in the form of square-wave pulses of low frequency (0.5–10 Hz). The set-up allows measurements of the electro-optical response at fixed wavelength while scanning the channel length, or measurements of local absorption spectra in the spectral range 4,000–16,000  $\text{cm}^{-1}$  (wavelength 2,500–625 nm) at any position along the SWNT channel as a function of applied voltage. The majority of the electro-optical experiments were conducted on separated 99% SC-SWNTs of average diameter  $D_{\text{av}} = 1.55 \pm 0.1$  nm, synthesized by the electric arc technique and obtained from Nanointegris (Figs 1–3, 5). Mixed SC- and metallic SWNTs, synthesized by laser ablation ( $D_{\text{av}} = 1.3 \pm 0.1$  nm) and the HiPCO process ( $D_{\text{av}} = 1.0 \pm 0.2$  nm), were obtained from Carbon Nanotechnologies. Predominantly SC-SWNTs ( $D_{\text{av}} = 0.8 \pm 0.1$  nm, CoMoCAT SG65 SWNTs) were obtained from SouthWest Nanotechnologies. Separated 99% metallic SWNTs of average diameter  $D_{\text{av}} = 1.55 \pm 0.1$  nm were obtained from Nanointegris and used as the transparent conducting gate electrode in the devices reported in Fig. 4. The ionic liquid (DEME-TFSI) was obtained from Kanto Corporation.

Received 10 September 2012; accepted 20 February 2013;  
published online 21 April 2013

## References

- Dresselhaus, M. S., Dresselhaus, G. & Avouris, P. *Carbon Nanotubes: Synthesis, Structure, Properties and Applications* (Springer-Verlag, 2001).
- Dresselhaus, M. S., Dresselhaus, G. & Jorio, A. *Carbon Nanotubes: Advanced Topics in the Synthesis, Structure, Properties and Applications* (Springer-Verlag, 2008).
- Avouris, P., Freitag, M. & Perebeinos, V. Carbon-nanotube photonics and optoelectronics. *Nature Photon.* **2**, 341–350 (2008).
- Freitag, M., Martin, Y., Misewich, J. A., Martel, R. & Avouris, P. Photoconductivity of single carbon nanotubes. *Nano Lett.* **3**, 1067–1071 (2003).
- Levitsky, I. A. & Euler, W. B. Photoconductivity of single-wall carbon nanotubes under continuous-wave near-infrared illumination. *Appl. Phys. Lett.* **83**, 1857–1859 (2003).
- Freitag, M. *et al.* Hot carrier electroluminescence from a single carbon nanotube. *Nano Lett.* **4**, 1063–1066 (2004).
- Itkis, M. E., Borondics, F., Yu, A. & Haddon, R. C. Bolometric infrared photoresponse of suspended single-walled carbon nanotube films. *Science* **312**, 413–416 (2006).
- Tarasov, M., Svensson, J., Weis, J., Kuzmin, L. & Campbell, E. Carbon nanotube based bolometer. *JETP Lett.* **84**, 267–270 (2006).
- Lee, J. U., Codella, P. J. & Pietrzykowski, M. Direct probe of excitonic and continuum transitions in the photocurrent spectroscopy of individual carbon nanotube p–n diodes. *Appl. Phys. Lett.* **90**, 053103 (2007).
- Mann, D. *et al.* Electrically driven thermal light emission from individual single-walled carbon nanotubes. *Nature Nanotech.* **2**, 33–38 (2007).
- Itkis, M. E., Yu, A. & Haddon, R. C. Single-walled carbon nanotube thin film emitter–detector integrated optoelectronic device. *Nano Lett.* **8**, 2224–2228 (2008).
- St-Antoine, B. C., Menard, D. & Martel, R. Single-walled carbon nanotube thermopile for broadband light detection. *Nano Lett.* **11**, 609–613 (2011).
- Wu, Z. *et al.* Transparent, conductive carbon nanotube films. *Science* **305**, 1273–1276 (2004).
- Gruner, G. Carbon nanotube films for transparent and plastic electronics. *J. Mater. Chem.* **16**, 3533–3539 (2006).
- Zhang, D. *et al.* Transparent, conductive, and flexible carbon nanotube films and their applications in organic light-emitting diodes. *Nano Lett.* **6**, 1880–1886 (2006).
- Zhang, M. *et al.* Strong, transparent, multifunctional, carbon nanotube sheets. *Science* **309**, 1215–1219 (2005).
- Kaempgen, M., Duesberg, G. S. & Roth, S. Transparent carbon nanotube coating. *Appl. Surf. Sci.* **252**, 425–429 (2005).
- Kavan, L. *et al.* Electrochemical tuning of electronic structure of single-walled carbon nanotubes: *in-situ* Raman and vis-NIR studies. *J. Phys. Chem. B* **105**, 10764–10771 (2001).
- Zukalova, M., Tarabek, J., Kalbac, M., Kavan, L. & Dunsch, L. *In situ* optical spectroelectrochemistry of single-walled carbon nanotube thin films. *J. Solid State Electrochem.* **12**, 1279–1284 (2008).
- Wang, F., Itkis, M. E. & Haddon, R. C. Enhanced electromodulation of infrared transmittance in semitransparent films of large diameter semiconducting single-walled carbon nanotubes. *Nano Lett.* **10**, 937–942 (2010).
- Perebeinos, V. & Avouris, P. Exciton ionization, Frank–Keldysh, and Stark effects in carbon nanotubes. *Nano Lett.* **7**, 609–613 (2007).
- Takenobu, T., Murayama, Y. & Iwasa, Y. Optical evidence of Stark effect in single-walled carbon nanotube transistors. *Appl. Phys. Lett.* **89**, 263510 (2006).
- Takenobu, T., Murayama, Y., Shiraishi, M. & Iwasa, Y. Optical observation of carrier accumulation in single-walled carbon nanotube transistors. *Jpn J. Appl. Phys.* **45**, L1190–L1192 (2006).
- Ham, M. H., Kong, B. S., Kim, W. J., Jung, H. T. & Strano, M. S. Unusually large Franz–Keldysh oscillations at ultraviolet wavelengths in single-walled carbon nanotubes. *Phys. Rev. Lett.* **102**, 047402 (2009).
- Granqvist, C. G. Electrochromic materials: out of a niche. *Nature Mater.* **5**, 89–90 (2006).
- Baetens, R., Jelle, B. P. & Gustavsen, A. Properties, requirements and possibilities of smart windows for dynamic daylight and solar energy control in buildings: a state-of-the-art review. *Solar Ener. Mater. Solar Cells* **94**, 87–105 (2010).
- Granqvist, C. G. Oxide electrochromics: an introduction to devices and materials. *Solar Ener. Mater. Solar Cells* **99**, 1–13 (2012).
- Jaksic, N. I. & Salahifar, C. A feasibility study of electrochromic windows in vehicles. *Solar Ener. Mater. Solar Cells* **79**, 409–423 (2003).
- Chen, J. *et al.* Solution properties of single-walled carbon nanotubes. *Science* **282**, 95–98 (1998).
- Matsunaga, R., Matsuda, K. & Kanemitsu, Y. Observation of charged excitons in hole-doped carbon nanotubes using photoluminescence and absorption spectroscopy. *Phys. Rev. Lett.* **106**, 037404 (2011).
- McEuen, P. L. & Park, J.-Y. Electron transport in single-walled carbon nanotubes. *MRS Bull.* **29**, 272–275 (2004).
- Yaish, Y. *et al.* Electrical nanoprobe of semiconducting carbon nanotubes using an atomic force microscope. *Phys. Rev. Lett.* **92**, 046401 (2004).

33. Kang, D. *et al.* Adsorption-induced conversion of the carbon nanotube field effect transistor from ambipolar to unipolar behavior. *Appl. Phys. Lett.* **86**, 093105 (2005).
34. Nosho, Y., Ohno, Y., Kishimoto, S. & Mizutani, T. Relation between conduction property and work function of contact metal in carbon nanotube field-effect transistors. *Nanotechnology* **17**, 3412–3415 (2006).
35. Chai, Y. *et al.* Low-resistance electrical contacts to carbon nanotubes with graphite interfacial layer. *IEEE Trans. Electron. Dev.* **59**, 12–19 (2012).
36. Ye, J. T. *et al.* Liquid-gated interface superconductivity on an atomically flat film. *Nature Mater.* **9**, 125–128 (2010).
37. Ueno, K. *et al.* Electric-field-induced superconductivity in an insulator. *Nature Mater.* **7**, 855–858 (2008).
38. Ueno, K. *et al.* Discovery of superconductivity in  $\text{KTaO}_3$  by electrostatic carrier doping. *Nature Nanotech.* **6**, 408–412 (2011).
39. Yuan, H. T. *et al.* High-density carrier accumulation in ZnO field-effect transistors gated by electric double layers of ionic liquids. *Adv. Funct. Mater.* **19**, 1046–1053 (2009).
40. Yuan, H. T. *et al.* Liquid-gated ambipolar transport in ultrathin films of a topological insulator  $\text{Bi}_2\text{Te}_3$ . *Nano Lett.* **11**, 2601–2605 (2011).
41. Ye, J. T. *et al.* Accessing the transport properties of graphene and its multilayers at high carrier density. *Proc. Natl Acad. Sci. USA* **108**, 13002–13006 (2011).

## Acknowledgements

This material is based on research sponsored by the Defense Microelectronics Activity (DMEA) (agreement no. H94003-10-2-1003). The US Government is authorized to reproduce and distribute reprints for Government purposes, notwithstanding any copyright notation thereon.

## Author contributions

F.W., M.E.I. and R.C.H. contributed to the original idea. M.E.I. and R.C.H. supervised the project. F.W. and M.E.I. designed and set up the experiment. F.W. performed the experiment. F.W., M.E.I., E.B. and R.C.H. contributed to the data analysis, interpretation of the results and preparation of the manuscript. M.E.I. and R.C.H. wrote the manuscript.

## Additional information

Reprints and permissions information is available online at [www.nature.com/reprints](http://www.nature.com/reprints). Correspondence and requests for materials should be addressed to R.C.H.

## Competing financial interests

The authors declare no competing financial interests.